Low-Loss, Narrowband Integrated Si₃N₄ Pulse Shaper for Quantum Photonic Applications

Lucas M. Cohen ¹, Karthik V. Myilswamy ¹, Navin B. Lingaraju ^{1,2}, and Andrew M. Weiner ^{1,*}

¹ School of Electrical and Computer Engineering and Purdue Quantum Science and Engineering Institute, Purdue University, West Lafayette, Indiana 47907, USA ² SRI International, 1100 Wilson Blvd. Suite 2800, Arlington, Virginia 22209, USA *amw@purdue.edu

Abstract: We demonstrate an optical pulse shaper in silicon nitride with spectral resolution on the order of a few GHz and line-by-line phase control for potential applications in quantum communications and networking. © 2021 The Author(s)

Optical pulse shaping is critical to a variety of classical [1] applications and is finding increasing use in the quantum space as well [2]. However, commercially available bench-top pulse shapers, which have been designed for classical lightwave communications, feature high insertion loss (\approx 6 dB) and limited wavelength resolution (\approx 20 GHz), limiting their utility in quantum applications. Integrated photonics has the potential to significantly reduce optical loss and, therefore, offer finer spectral resolution than is currently possible with discrete components. In this work, we demonstrate a low-loss, narrowband integrated optical pulse shaper on a silicon nitride (Si₃N₄) platform. Compared to prior work [3, 4], our pulse shaper features finer resolution (\approx 2 GHz), thereby enabling dense packing of multiple frequency channels. With successful demonstration of several other on-chip components such as photon pair sources [5] and electro-optic modulators [6], one can envision the integration of such high-resolution pulse shapers into large-scale photonic circuits for quantum information processing.

Our integrated pulse shaper used was fabricated by LIGENTEC on their AN800 platform [7], which includes an 800 nm thick $\mathrm{Si_3N_4}$ layer (see Figure 2(a)). Each spectral channel in the pulse shaper includes a microring filter to download an incoming spectral channel, a phase shifter to provide line-by-line phase control, and a second microring filter to upload the modified spectral channel onto a common output bus waveguide [8]. The 40 μm radius microring filters have free spectral ranges (FSR) of roughly 570 GHz. The thermo-optic phase shifter is an 800 μm -long waveguide with Al-based metal layer above. Each microring filter has a metal heater for trimming of the resonant wavelength. The entire pulse shaper includes six spectral channels and occupies a total footprint of 3.55×0.45 mm.

The silicon nitride chip, including electrical and optical probes are shown in Figure 1(a). While the full-width half-maximum (FWHM) of each microring filter is ≈ 3.5 GHz, the cascading of two such filters in each pulse shaper channel leads to channel bandwidth of ≈ 2.5 GHz. To characterize the response of the pulse shaper, including inline phase control, each pulse shaper is included within one arm of a Mach-Zehnder interferometer (MZI) with a straight waveguide in the other arm. The pulse shaper is designed to permit access to the through port responses of both the upload and download filters, with spectra for a single download filter shown in Figure 1(b) for various levels of electrical bias up to failure. Owing to the low resistivity of the metal layer, tuning of the resonant wavelength over only ≈ 1.2 nm, or a quarter FSR, is possible.

By tuning the upload and download microring filters such that the resonant wavelengths within a channel of the pulse shaper are aligned, one can characterize the performance of inline phase control from interference observed at the output of the MZI. The analytical and experimental responses for various phase shifts applied to the pulse shaper channel are shown in Figures 1(c) and (d), respectively. There is agreement between theory experiment

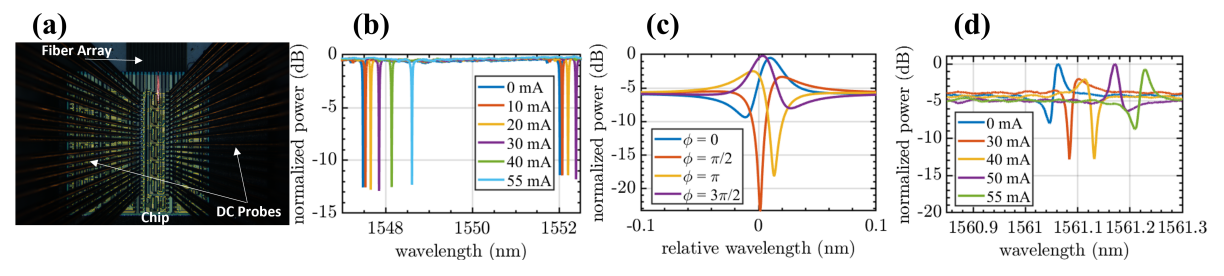


Fig. 1. (a) Experimental setup including DC probes, optical fiber array, and Si_3N_4 chip. (b) Spectra from thermal tuning of a single microring within a channel. (c) Analytical response of MZI structure with applied phase ϕ from the phase shifter. (d) Experimental MZI response with various applied currents to the thermo-optic phase shifter.

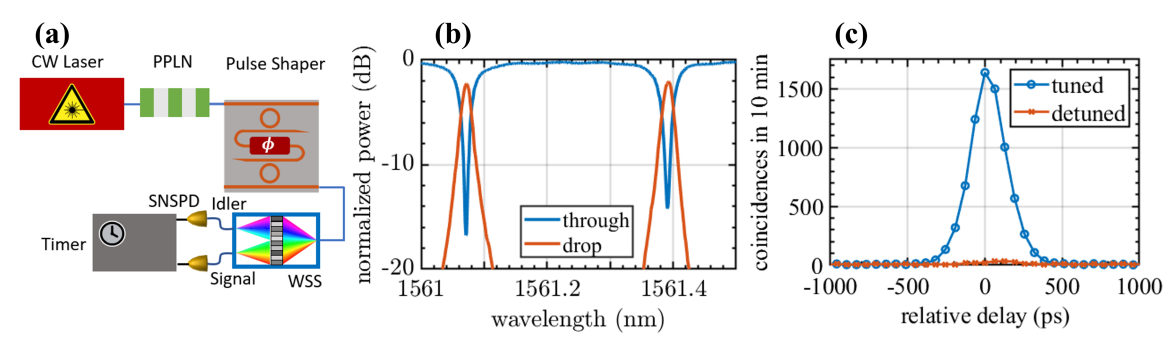


Fig. 2. (a) Diagram of the experimental setup (only single channel shown). (b) Two-channel shaper response. (c) Coincidence measurements for tuned and detuned shaper channels (details in text).

with the exception of a consistent redshift as the power delivered to the phase shifter increases in the experiment. This is attributed to symmetric heating of the upload and download microrings owing to thermal crosstalk with the phase shifter. These traces highlight that a single channel of our pulse shaper can isolate a narrowband spectral channel and introduce the prescribed phase.

To validate pulse shaper operation in the context of quantum photonics, we configure two channels of the pulse shaper to carve a broadband down-conversion spectrum as outlined in Figure 2(a). Time-frequency–entangled photons are generated via spontaneous parametric down-conversion by pumping a periodically poled lithium niobate waveguide (PPLN) with a tunable continuous-wave laser (CW) at ≈ 780 nm. The Si₃N₄ chip is fixed at 29.5 C° by a thermo-electric cooler and two channels of the pulse shaper are detuned from the remaining four channels in the system and set 40 GHz apart from one another, shown in Figure 2(b). Drop port loss for a single pulse shaper channel is estimated to be 1.75 dB.

The PPLN waveguide is pumped such that the broadband (≈ 5 THz) biphoton spectrum is centered midway between the two pulse shaper channels used in the experiment. 2.5 GHz spectral slices (equal to the single channel FWHM) of the signal and idler are carved using this two-channel pulse shaper. These spectrally carved signal and idler photons are routed to a bench-top wavelength selective switch (WSS) to separate them for coincidence detection with superconducting nanowire single-photon detectors (SNSPDs). The coincidence results are shown in Figure 2(c) showing a temporal FWHM of ≈ 0.3 ns, which is consistent with the spectral badnwidth of the carved photons ($\Delta t \approx 1/\Delta v_{FWHM}$). We also red detune the high-wavelength channel by 10 GHz and repeat coincidence measurements to verify that events are only recorded for energy-matched spectral slices. As seen from Figure 2(c), detuning the single channel virtually eliminates coincidences. The tuned and 10 GHz detuned coincidence-to-accidental ratios (CARs) are 205 and 4, respectively. The significant reduction in the CAR in the detuned case demonstrates fast roll-off in the pulse shaper response. The fine spectral resolution of our pulse shaper allows for time-resolved measurement of the biphoton temporal correlation, which otherwise would have been averaged owing to detector jitter (≈ 110 ps).

In sum, we have demonstrated a low-loss, narrowband integrated Si_3N_4 pulse shaper using a commercial foundry. In subsequent work, we will improve system performance by minimizing thermal crosstalk between on-chip components to ensure straightforward electronic control of the full system. We anticipate that pulse shapers with fine control over the spectral bandwidth will find use in applications to manipulate spectral phase of narrow linewidth quantum signals and will also be of interest to the broader photonics research community.

This work was supported in part by National Science Foundation (ECCS-1809784, ECCS-2034019) and Department of Energy (STTR grant DE-SC0021517) through Freedom Photonics In our experiments, we use a Maple Leaf optical probe station [9] to optically and electrically probe our Si_3N_4 chip. We acknowledge Saleha Fatema, Cong Wang, and Jonas Flueckiger for helpful discussions.

References

- 1. A. M. Weiner, Opt. Commun. **284**, 3669-3692 (2011).
- 2. H.-H. Lu, et al., IEEE Photon. Technol. Lett. 31, 1858 (2019).
- 3. A. Agarwal, et al., J. Light. Technol. 24, 77–86 (2006).
- 4. R. P. Scott, et al., Opt. Express 15, 9977-9988 (2007).
- 5. P. Imany, et al., Opt. Express 26, 1825 (2018).
- 6. D. Zhu, et al., Adv. Opt. Photonics 13, 242-352 (2021).
- 7. LIGENTEC. Online. Available: https://www.ligentec.com/ligentec-foundry/
- 8. J. Wang, et al., Nat. Commun. 6, 5957 (2015).
- 9. Maple Leaf Photonics. Online. Available: https://www.mapleleafphotonics.com/